W. Eißler & H. Bestek

Wall-Temperature Effects on Transition in Supersonic Boundary Layers Investigated by Direct Numerical Simulations

Abstract

The effects of different wall-temperature conditions on laminar-turbulent transition in Mach 4.8 flat-plate boundary layers at flight conditions are investigated using spatial direct numerical simulations. Using radiation adiabatic wall temperature conditions, the simulations allow, for the first time, to calculate the realistic increase of the wall temperature caused by the fundamental-type transition process.

Introduction

Heat loads resulting from friction and compression of air represent a key problem of hypersonic flight. The wall temperature is determined by the heat balance between heat transfer to the surface due to aerothermal loads, heat radiated from the surface, and heat conducted within and stored in the vehicle structure. For the design of hypersonic vehicles, a good estimate of the resulting aerothermal loads and wall temperatures is of vital importance, which requires the accurate prediction of boundary-layer transition and turbulence. However, the existing transition prediction methods and turbulence models needed for this task still contain an unknown degree of uncertainty as detailed experiments do not exist for such flow conditions.

Transition to turbulence in supersonic and hypersonic boundary layers is still a poorly understood problem. While the first initial stage of the transition process, i.e. the growth of linear disturbances is adequately described by compressible linear stability theory (Mack, 1969; Mack, 1984), the subsequent nonlinear stages are widely unknown, as there is no guidance from experiments. Transition experiments in high-speed boundary layers are very difficult to perform. Therefore, linear stability theory is widely used to determine the important parameters affecting transition and their trends, that is, whether and how much a change of some parameter is stabilizing or destabilizing. In recent years, direct numerical simulations have shown their capability to be used as a new tool in high-speed transition research, as they can be applied in situations where experiments seem impossible to perform. This is demonstrated in the present paper for transition at flight conditions.

In the past several years many efforts have been made experimentally, theoretically, and numerically in order to gain a better understanding of supersonic

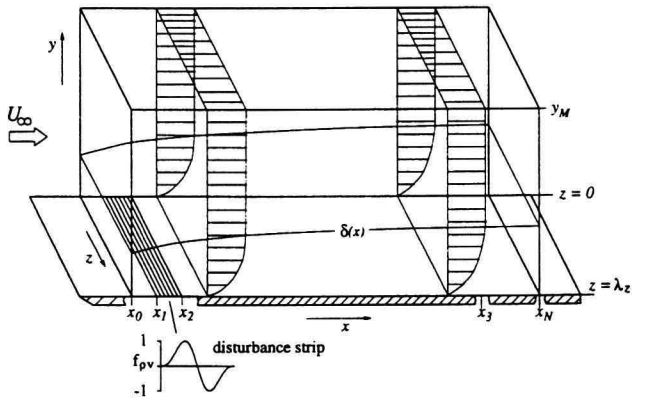

Figure 1: Sketch of the integration domain and the disturbance input.

transition, which is indispensable for the development of reliable transition prediction methods and turbulence models for compressible boundary layer flows. However, most of these studies were concerned with transition at wind-tunnel temperature conditions, aiming to understand and model the phenomena observed in a few detailed experiments. The effect of high temperatures on transition, as encountered by a hypersonic vehicle in the atmosphere, are still completely unknown.

In this paper, we present results from several simulations to study the effect of different wall-temperature conditions on transition in Mach 4.8 flat-plate boundary layers at flight conditions. The flat-plate is a representative model for the boundary-layer flow on a hypersonic aerospace plane at flight conditions at 25 km altitude. Using radiation adiabatic wall-temperature conditions the simulations allow, for the first time, to calculate the realistic streamwise increase of the wall temperature caused by the transition process.

Numerical model

Laminar-turbulent transition phenomena in a supersonic boundary-layer flow over a flat plate are investigated by spatial direct numerical simulations based on the complete, three-dimensional Navier-Stokes equations, the continuity equation, the energy equation, and the thermodynamic equation of state for a compressible perfect gas in equilibrium. The equations are used in conservative form for the variables $\rho, \rho u, \rho v, \rho w$ and ρe (Eißler & Bestek, 1995). The integration domain shown in Fig. 1 extends from $x = x_0$ to $x = x_N$ in the streamwise x-direction, with x_0 being the downstream distance from the leading edge of the flat plate. In the wall-normal y-direction, the integration domain extends from $y = 0$ to $y = y_M$ and typically covers several boundary-layer thicknesses. In the spanwise z-direction, the flow is assumed to be periodic with the domain extending from $z = 0$ to $z = \lambda_z$, where λ_z is a fundamental spanwise wavelength which can be chosen arbitrarily.

The governing equations are normalized with the freestream values of the velocity, the temperature, and the density. Furthermore the global Reynolds number $Re = \frac{\rho^\star_\infty u^\star_\infty L}{\mu^\star_\infty} = 10^5$ is used, where the superscript $\star$ denotes the dimensional quantities, and thus the local Reynolds number is defined as $Re_x = \frac{\rho^\star_\infty u^\star_\infty x^\star}{\mu^\star_\infty} = x \cdot Re$. The thermodynamic properties are approximated as a calorically perfect gas with a constant Prandtl number $Pr = 0.71$, a constant ratio of the specific heats $\kappa = 1.4$, and Sutherland's law for the dynamic viscosity μ. For all simulations discussed in this paper the freestream Mach number is $Ma = 4.8$.

Numerical method

The numerical method is based on an explicit Runge-Kutta scheme of fourth-order accuracy in time. In x- and y-direction finite-difference approximations of fourth-order accuracy are used, and in the spanwise z-direction, a spectral (Fourier) approximation is employed. The grid is equally spaced in the x- and y-directions.

The numerical procedure is decomposed into two steps: the calculation of a steady, two-dimensional, laminar boundary layer by solving the two-dimensional form of the governing equations (Eißler & Bestek, 1995), and the calculation of the evolution of two- and three-dimensional disturbances which are introduced into the laminar boundary layer by localized periodic blowing and suction through a narrow disturbance strip at the plate surface (see Fig. 1). The reaction of the boundary layer to this periodic forcing, i.e. the spatial downstream development of the disturbance waves, is then simulated numerically.

Similar to the linear stability theory (LST) and the PSE-method, the flow is decomposed into the steady, laminar base flow Φ_B and the disturbance flow Φ', which consists of steady and unsteady disturbances. This procedure allows for the calculation of two- and three-dimensional harmonic waves as well as for a steady mean-flow distortion, which represents the transitional mean deviation from the laminar boundary layer.

Boundary conditions

Boundary conditions have to be defined for the steady, laminar two-dimensional base flow as well as for the three-dimensional disturbance flow. For the disturbance flow, the boundary conditions have to be valid for high-frequency harmonics as well as for the steady mean-flow distortion.

At the *inflow boundary* $x = x_0$ an undisturbed steady base flow, as obtained from the solution of the compressible boundary-layer equations, is assumed. No disturbances are allowed here. At the *outflow boundary* $x = x_N$ the second derivatives with respect to x are set to zero for the base flow. For the disturbance flow, a procedure similar to the "relaminarization technique" developed by (Kloker, Konzelmann & Fasel, 1993) is used (Eißler & Bestek, 1995). At

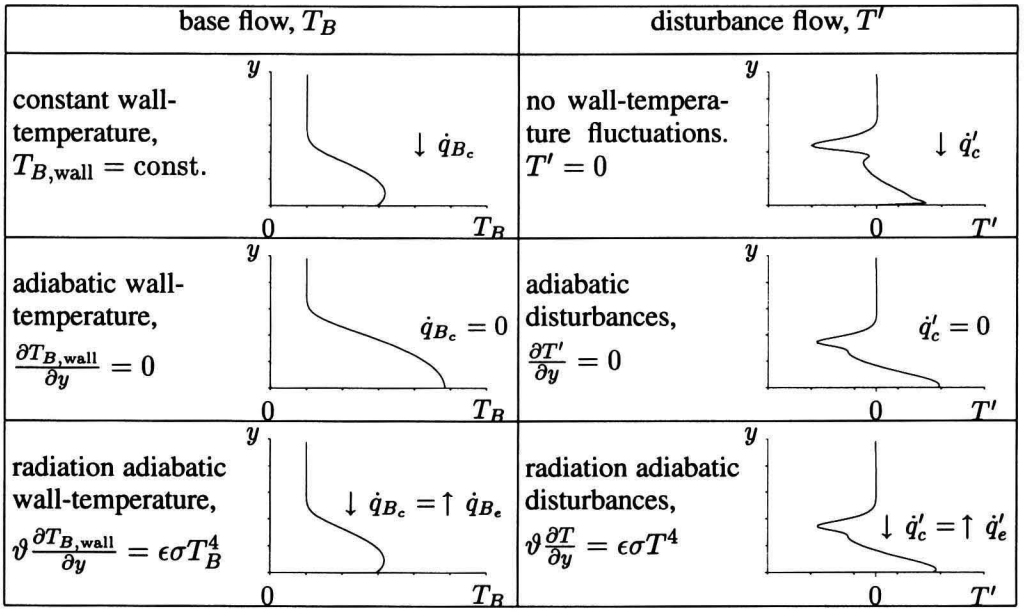

Figure 2: Shape of the temperature distribution for different wall temperature conditions for the base flow (left side) and for the disturbance flow (right side).

the *lateral boundaries* $z = 0$ and $z = \lambda_z$ the disturbances are assumed to be periodic with the spanwise wavenumber β. At the *freestream boundary* $y = y_M$ an inviscid flow is assumed. For the base flow as well as for the disturbance flow, non-reflecting characteristic conditions are used. At the *wall* $y = 0$ all velocity components are zero, the pressure is calculated from the y-momentum equation, density is determined from the equation of state, and internal energy is calculated from its definition.

No unique condition can be defined for the wall temperature, as we do not solve the Poisson heat equation within the wall, neither for the steady base-flow nor for the disturbance flow. Therefore, it is useful to know the temperature range that can occur principally. The conditions for the base flow and the disturbance flow are discussed separately, and are sketched in Fig. 2.

Without artificial heating, the maximum base-flow temperature is the recovery temperature of an adiabatic wall. For wind-tunnel experiments, the adiabatic-wall condition is often used. For a flight vehicle moving at Mach 5 in the atmosphere, the adiabatic wall temperature can reach some 1000 K. Of course, in reality wall heat conduction and radiation will lead to a cooled wall. These kinds of cooling can be approximated in the simulation by a constant wall temperature, or a radiation adiabatic wall, respectively.

For the disturbance flow, the situation becomes more difficult, as the wall-

temperature condition must be valid for the mean-flow distortion and the high-frequency disturbances. The condition almost always used, is the assumption of zero temperature disturbances at the wall. This condition seems to be reasonable as it is hardly conceivable that the wall temperature may fluctuate with frequencies in the order of 100 kHz. However, when applying this condition, the (mean) wall-temperature remains on its steady laminar value, even at the late stages of transition in DNS. This condition implies the largest temperature gradient that can be obtained at the wall and therefore the largest wall heat flux. In reality, this behaviour could be achieved by a wall with an infinite specific heat, where any heat flux does not affect the wall temperature. The opposite can be obtained using adiabatic temperature disturbances. Now, no heat flux penetrates into the wall but the temperature fluctuations are maximum. This would be true, if the the specific heat of the wall was zero. As a consequence, it is obvious that in reality the temperature condition must be somewhere between these two extremes, as neither the temperature fluctuations nor the heat flux should be zero at the wall.

A condition that contains both, temperature fluctuations and heat flux, is the radiation adiabatic wall. Here, the convective heat flux penetrating into the wall is equal to the radiative heat flux from the wall, and we get $\vartheta^\star \dfrac{\partial(T_B^\star + T^{\star\prime})}{\partial y^\star} = \epsilon\,\sigma\,(T_B^\star + T^{\star\prime})^4$, with the Stefan-Boltzmann constant σ, the emissivity constant ϵ of the surface and the thermal conductivity coefficient ϑ. The typical shapes of the temperature distributions in y-direction for the base flow and the disturbance flow, respectively, are plotted in Fig. 2 for the six boundary conditions discussed before.

Results

Effects of wall-temperature conditions

To investigate the effects of the wall temperature on transition, simulations were performed for four cases using different boundary conditions. In all cases, the freestream temperature was assumed to be $T^\star_{B,\infty} = 220$ K, corresponding to atmospheric conditions at 25 km altitude. The frequency of the forced disturbances was $F = 10 \cdot 10^{-5}$ and the integration domain was located inside the second-mode unstable region for that frequency. At the disturbance strip, a two-dimensional wave (mode (1,0)) and a pair of three-dimensional waves (mode (1,1)) were forced with the same frequency, in order to initiate the fundamental-type transition process. Here, the two- and three-dimensional disturbance components are denoted as modes (h, k), where h stands for the frequency in integer multiples of the fundamental frequency and k denotes multiples of the spanwise wave number. The resolution of the simulations was chosen to be sufficient for the initial nonlinear disturbance development. In agreement with a previous study (Eißler & Bestek, 1995), where we considered simulations $\mathcal{A}$ to $\mathcal{D}$, the four cases were denoted by $\mathcal{B}$,$\mathcal{C}$,$\mathcal{E}$, and $\mathcal{F}$. The parameters of the four simulations are given in Fig. 3.

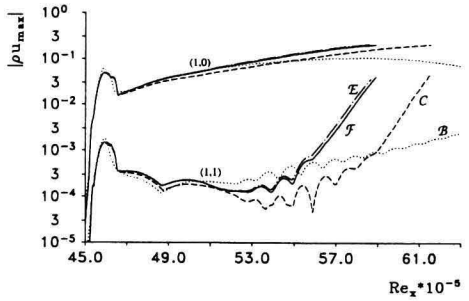

	$\mathcal{B}$	$\mathcal{C}$	$\mathcal{E}$	$\mathcal{F}$
$T^\star_\infty$ [K]	220			
$T^\star_w$ [K]	1065	650		647-633
T'_w	0		adiab.	rad. ad.
$F_{1,0}$	$10 \cdot 10^{-5}$			
$F_{1,1}$	$10 \cdot 10^{-5}$			
Trans. mech.	fundamental breakdown			

Figure 3: Amplitude maxima $|(\rho u)'_{h,k}|$, and simulation parameters of the four simulations for fundamental resonance at atmospheric conditions. (····· $\mathcal{B}$, – – – – $\mathcal{C}$, – · – · – · $\mathcal{E}$, ——— $\mathcal{F}$)

In simulation $\mathcal{B}$, the base flow was assumed to be adiabatic ($T^\star_{B,\text{wall}} = 1065$ K) and the temperature disturbances were set to zero at the wall. This is traditionally assumed in LST. The effect of a cooled boundary layer can be studied with simulation $\mathcal{C}$, were a constant wall temperature ($T^\star_{B,\text{wall}} = 650$ K) was used. Again, the temperature disturbances were set to zero. The effect of adiabatic and radiation adiabatic disturbances can be studied with simulations $\mathcal{E}$ and $\mathcal{F}$, respectively. In simulation $\mathcal{E}$ the base-flow wall temperature was held constant ($T^\star_{B,\text{wall}} = 650$ K), and adiabatic conditions were used for the temperature disturbances. In simulation $\mathcal{F}$ radiation adiabatic conditions were used for the base flow ($T^\star_{B,\text{wall}}$ between 647 and 633 K), and for the disturbance flow.

It is well known from LST Mack, 1984) that wall cooling destabilizes second mode disturbances. Therefore, it is obvious that the amplitude of the two-dimensional, fundamental disturbance $(\rho u)_{1,0}$ of case $\mathcal{C}$ increases faster than the corresponding amplitude of case $\mathcal{B}$, as can be seen in Fig. 3. When the wall temperature disturbances are adiabatic or radiation adiabatic ($\mathcal{E}$,$\mathcal{F}$) instead of being zero ($\mathcal{C}$), the two-dimensional amplitudes $(\rho u)_{1,0}$ grow even faster. Thus, the onset of resonance in simulations $\mathcal{E}$ and $\mathcal{F}$ occurs upstream compared to simulation $\mathcal{C}$. In simulation $\mathcal{B}$, the two-dimensional disturbance reaches a maximum and decays further downstream. Consequently, the secondary amplification of the three-dimensional, fundamental disturbance $(\rho u)_{1,1}$ for case $\mathcal{B}$ is weak compared to the simulations $\mathcal{C}$,$\mathcal{E}$, and $\mathcal{F}$.

Comparing simulations $\mathcal{C}$ and $\mathcal{E}$, where minimum and maximum wall temperature fluctuations were assumed, it becomes clear, that transition predictions based on stability results using the traditional non-fluctuating conditions are too optimistic.

Fundamental transition for a radiation adiabatic wall

To investigate the effect of the most realistic radiation adiabatic wall-temperature condition in a transitional flow, simulation $\mathcal{F}$ was repeated with a better resolution in time and space. The streamwise amplitude developments of the 3-D

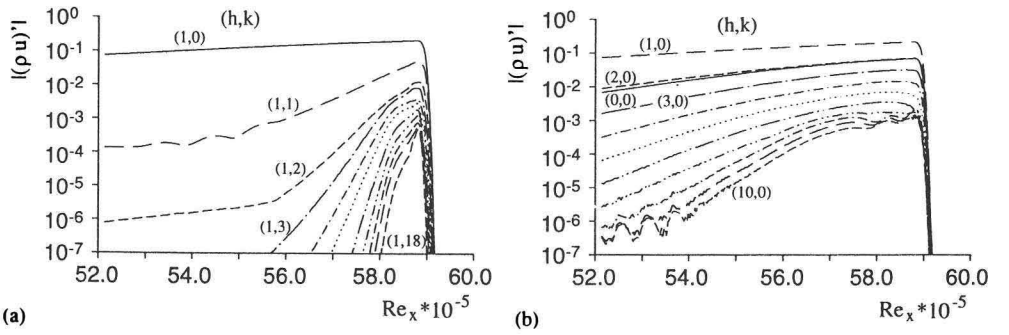

Figure 4: Amplitude development of $|(\rho u)'|$ for (a) 3-D disturbances with fundamental frequency (modes (1,k)), and for (b) 2-D disturbances (modes (h,0)).

disturbances with fundamental frequency $|(\rho u)_{1,k}|$, and the 2-D disturbances $|(\rho u)_{h,0}|$ are shown in Fig. 4. The fundamental 2-D disturbance (mode (1,0)) increases continuously caused by the primary instability. At $Re_x \approx 55.5 \cdot 10^5$ a secondary growth of the 3-D disturbances starts, and the growth rate increases for larger spanwise wave numbers. Here is the onset of fundamental resonance is found. At $Re_x \approx 58.5 \cdot 10^5$, where the resolution of the numerical simulation begins to be insufficient, the amplitudes of the leading 2-D disturbances are still higher than the 3-D disturbances. Thus, the initial transitional stages are dominated by 2-D disturbances, the effects of 3-D disturbances become important only in the late transitional stages, and the transitional region is small compared to the unstable region, which begins at $Re_x \approx 46 \cdot 10^5$.

In Fig. 5, the corresponding streamwise evolution of the boundary-layer thickness δ, the displacement thickness δ_1, the momentum thickness δ_2, the shape factor H_{12}, and the skin friction coefficient c_f are plotted. The location and the effect of the numerical damping zone near the outflow can be clearly identified for $Re_x > 59 \cdot 10^5$, where the boundary layer parameters are ramped down to their laminar values. At $Re_x \approx 57 \cdot 10^5$ the shape factor begins to deviate remarkably from its laminar value, and the skin friction starts to increase faster. Here the onset of the boundary-layer transition of this simulation occurs.

The radiation adiabatic wall-temperature condition was developed to study the effect of transition on the mean heat flux and the mean temperature development at the wall. In Fig. 6, isolines of the mean temperature gradient $\partial T/\partial y$ (which is proportional to the mean heat flux), and the mean wall-temperature distribution at the plate surface are shown. The spanwise distributions of both parameters are almost two-dimensional, and almost constant up to $Re_x \approx 57.5 \cdot 10^5$. Further downstream both parameters increase rapidly, and a three-dimensional deformation can be observed, which has a similar shape for both parameters. The fastest growth is observed in the plane $\lambda_z = 0.5$, which is the well known "Peak Plane" of fundamental transition in incompressible boundary layers (Kachanov *et al.*, 1985). These results demonstrate the capability of

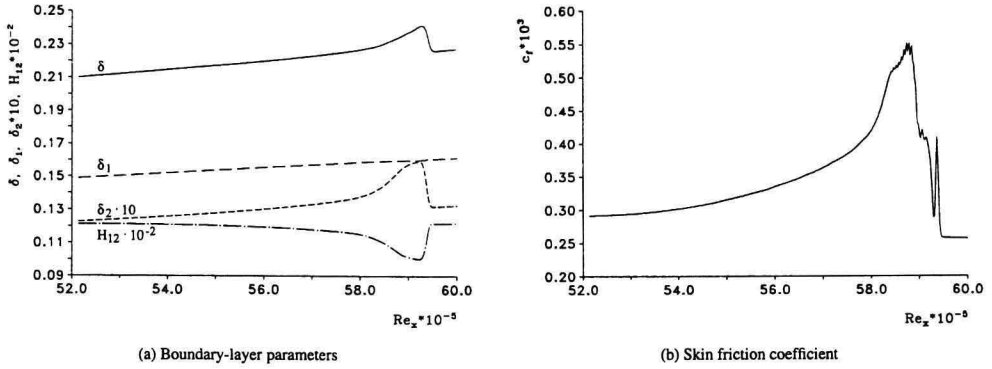

(a) Boundary-layer parameters (b) Skin friction coefficient

Figure 5: Streamwise evolution of the mean boundary-layer parameters δ, δ_1, δ_2 and H_{12}, and the mean skin-friction coefficient c_f.

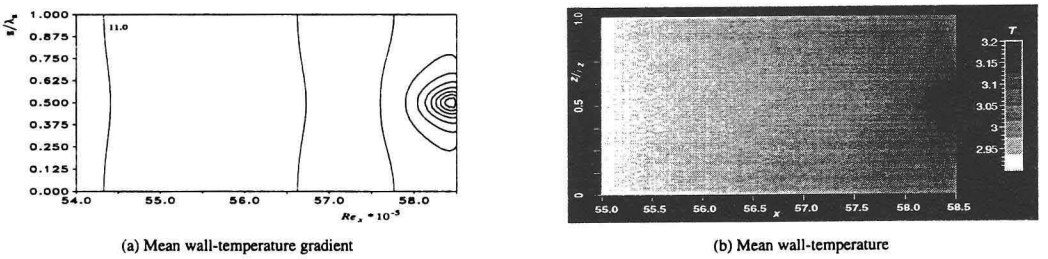

(a) Mean wall-temperature gradient (b) Mean wall-temperature

Figure 6: Distribution of the mean wall-temperature gradient ($\Delta\partial\langle T\rangle/\partial y = 1.0$), and of the mean wall-temperature.

the newly developed radiation-adiabatic wall-temperature condition for the disturbances to calculate the increase of the mean wall temperature in the late stages of transition, combined with a similar increase of the mean heat flux at the wall. This was not achieved in earlier DNS.

Conclusions

In the present paper, three different boundary conditions for the wall temperature to be used in spatial direct numerical simulations were discussed. The conditions were applied to the mean, laminar base flow and to the disturbance flow in a supersonic boundary layer. It was shown that the classic non-fluctuating wall-temperature disturbance condition produces the largest possible heat flux at the wall but the mean wall temperature does not change its laminar value, even

in the late stages of transition. The opposite boundary condition was demonstrated to be the assumption of adiabatic disturbances, where the temperature disturbances are maximum but the heat flux diminishes to zero. This condition led to a significantly lower transition Reynolds number than the non-fluctuating temperature condition for the investigated second-mode disturbances. A more realistic condition, the radiation adiabatic wall, was developed and applied. The resulting increase of the mean wall temperature and the mean heat flux at the wall using this condition was shown for fundamental transition in a flat-plate boundary layer at Mach 4.8 at flight conditions.

Acknowledgement

This work was supported by the Deutsche Forschungsgemeinschaft (DFG) Bonn-Bad Godesberg, FRG, as part of SFB 259.

References

Eißler, W. & Bestek, H. 1995 – Numerical simulations of initial transition in Mach 4.8 boundary layers at wind-tunnel and flight conditions. *Z. Flugwiss. Weltraumforsch.* **19**, 228–235.

Kachanov, Y., Kozlov, V., Levchenko, V. & Ramazanov, M. 1985 – On nature of K-Breakdown of a laminar boundary layer. New experimental data, *In* V. Kozlov, ed., Laminar-Turbulent Transition, Springer-Verlag, Berlin, pp. 61–73.

Kloker, M., Konzelmann, U. & Fasel, H. 1993 – Outflow boundary conditions for spatial Navier-Stokes simulations of transition boundary layers. *AIAA J.* **31**, 620–628.

Mack, L. 1969 – Boundary layer stability theory, Technical Report 900-277, Rev. A, Jet Propulsion Laboratory, Pasadena, CA.

Mack, L. 1984 – Boundary-layer linear stability theory, *In* R. Michel, ed., 'Special Course on Stability and Transition of Laminar Flow', AGARD-Report-709, pp. 3.1–3.81.

Authors' address

Institut für Aerodynamik und Gasdynamik,
Universität Stuttgart,
D-70550 Stuttgart, Germany.